Mechanisms of near-ultraviolet, nanosecond-pulse–laser damage in HfO_2/SiO_2 – based multilayer coatings

S. Papernov

Laboratory for Laser Energetics, University of Rochester, Rochester, NY 14623-1299, USA

**Corresponding author: spap@lle.rochester.edu*

Received December 8, 2012; accepted January 13, 2013; posted online May 10, 2012

The possible role of metal clusters and electronic defects in the near-ultraviolet, nanosecond-pulse–laser damage in HfO_2/SiO_2-pair – based coatings is analyzed using experimental results on absorption and damage in HfO_2 monolayers with and without artificially introduced Hf nanoscale absorbers. These studies reveal a damage mechanism specific to HfO_2/SiO_2 pair combination comprised of a high-melting-point material (HfO_2), where absorption starts, and a lower-melting-point material (SiO_2), where absorption can be initiated upon reaching the critical temperature. Based on this analysis we discuss possible modifications to coating designs and desirable properties of high- and low-index materials that might lead to improve nanosecond, near-ultraviolet laser-damage performance.

OCIS codes: 140.0140, 310.0310, 160.0160.

doi: 10.3788/COL201311.S10703.

HfO_2/SiO_2 based multilayer coatings prepared by electron-beam deposition (EBD) are among the most frequently used coatings for near-ultraviolet (near-UV), high-power, and high-energy laser applications. Nanosecond-pulse–laser damage performance of these coatings is crucial for the successful operation of fusion-scale lasers working in the near-UV range and using corresponding transport optics. Further deterministic improvements in coating-damage thresholds greatly depend on clarification of the damage mechanism. The consensus exists that initial absorption leading to damage starts in the high-index HfO_2 layers. Current EBD of HfO_2 layers uses Hf metal as a starting material, which ensures a stable deposition that will result in good homogeneity and low density of micrometer-scale localized defects. Nevertheless, high-resolution damage-morphology studies[1] have demonstrated that near-UV absorption and damage in these coatings are initiated at much-smaller, isolated, nanometer-scale absorbing regions with still-unknown chemical composition and physical properties. In this work, we consider two probable sources of damage initiation: few-nanometer–sized Hf metal clusters and high-density areas of electronic defects. The former can be produced during evaporation from the molten metal pool; the latter (electronic defects) exist even in a bulk form[2] of HfO_2 and may have much-higher densities in thin films at grain boundaries, including boundaries with SiO_2 low-index layers. The possible role of clusters and electronic defects is analyzed using experimental results on absorption and damage in HfO_2 monolayers with and without artificially introduced Hf metal nanoclusters. These studies suggest a damage mechanism specific to HfO_2/SiO_2 pair combination comprised of a high-melting-point material (HfO_2), where absorption starts, and a lower-melting-point material (SiO_2), where absorption can be initiated upon reaching the critical temperature. Based on this analysis, we discuss possible modifications to coating designs and desirable properties of high- and low-index materials that might lead to improve nanosecond, near-UV laser-damage performance.

In the case of HfO_2/SiO_2 multilayers, HfO_2 is the material where absorption starts and eventually leads to damage. Numerous studies of 351-nm, nanosecond-pulse damage in HfO_2 and SiO_2 monolayers show much-lower damage thresholds for HfO_2 layers as compared to SiO_2 layers[3]. The band-gap comparison for these two materials (5.6 and 8.9 eV, respectively) also favors absorption and ionization of HfO_2 material in the case of irradiation by photons with 3.55 eV of energy. Nevertheless, as will be shown later, in coatings based on HfO_2/SiO_2 pairs, the energy deposition and the damage process are not confined to HfO_2 and actively involve SiO_2 material. The key to understanding damage initiation is linked to unambiguous identification of the nature and properties of absorption sources. Two most-probable candidates are Hf metal nanoclusters and high-density areas of electronic defects, such as electronic surface states at the columnar coating grain boundaries. The former formation is possibly due to the use of Hf metal as a starting material for EBD. Comparing the laser-damage behavior of HfO_2 monolayers with and without from 1- to 3-nm–sized gold particles as embedded artificial absorbers[4] suggested that, in the case where Hf nanoclusters are responsible for damage initiation, their size should not exceed a few nanometers. Concerning electronic defects, first-principle calculations[2] show the presence of electronic-defect states inside the HfO_2 bandgap (Fig. 1) that can initiate the generation of free electrons by absorption of 351-nm (3.55-eV) light. Due to coating inhomogeneous columnar structure, high-density areas of these defects may be also responsible for localized absorption and damage. Very small sample volumes along with the nanometer scale of these absorbers present a significant challenge for characterization of their chemical content, physical properties, and distribution in the host material. In this work, we used a photothermal heterodyne imaging (PHI) technique[5,6] to characterize the absorber distribution in the material by measuring spatially resolved absorption with submicrometer resolution. This technique was also applied to an analysis of the laser-damage morphology, and PHI maps were

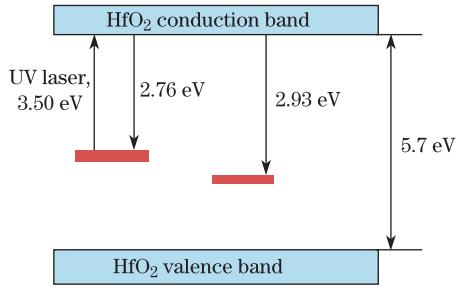

Fig. 1. Energy level diagram for defect states in bulk HfO_2 (as per Ref. [2]).

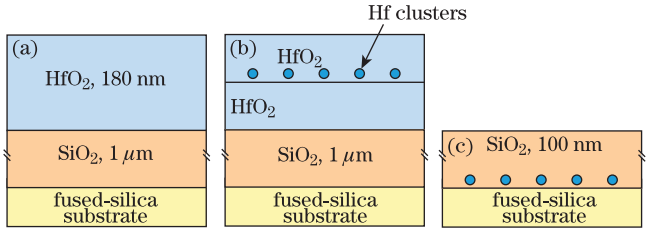

Fig. 2. Schematic of the thin-film samples. (a) HfO_2 sample without Hf particles; (b) HfO_2 sample with embedded Hf particles; (c) SiO_2 sample with embedded Hf particles.

correlated with topography obtained using atomic force microscopy (AFM).

Different types of thin-film monolayer samples used in this study are depicted in Fig. 2.

HfO_2 thin-film samples of 1-wave optical thickness (~180 nm) for PHI experiments were prepared on fused-silica substrates coated in the same coating run with a 1-μm-thick SiO_2 layer to insulate them from defects introduced by the polishing process (Fig. 2(a)). The conventional EBD rate for HfO_2 was 0.12 nm/s and the oxygen pressure was 8×10^{-5} Torr. In addition, 1/4-wave (~45-nm)-thick HfO_2 samples were deposited for PHI signal versus film-thickness variation studies. Figure 3 shows a 355-nm E-field intensity distribution assuming normal-incidence plane-wave approximation. One can find intensity peaks at both interfaces and in the bulk of 1-wave film and only one peak at the HfO_2/SiO_2 interface of 1/4-wave film. This information is taken into account when evaluating the interfacial absorption contribution to the PHI signal.

To investigate the possible role of small Hf metal clusters in the damage process, HfO_2 films with artificially introduced Hf clusters were manufactured (Fig. 2(b)). For this purpose, in the first coating run, samples were prepared similarly to the method described above with the only difference being that the HfO_2-layer thickness was 1/2 wave (90 nm) instead of 1 wave. As a second step, Hf metal clusters were deposited onto the HfO_2 film surface using through-thin-film ablation (TTFA)[7]. Ablation of 10-nm-thick Hf metal film was performed in a 0.5-Torr Ar atmosphere using nanosecond pulses from a 248-nm KrF laser. Hf cluster deposition for each shot was characterized (Fig. 4) using transmission electron microscopy (TEM) of witness samples placed adjacent to the HfO_2 film sample in the same target plane. Analysis of the TEM images showed that the absolute majority of Hf clusters had a diameter in the range of 1 – 5 nm with an average separation of ~20 nm, which corresponded to an areal density of $\sim 10^3 \mu m^{-2}$. These images also showed the presence of large particles of from 20- to 150-nm size and an average areal density of $\sim 0.4 \mu m^{-2}$. Such areal density is low enough not to interfere with the investigation of absorption caused by small clusters, but it is high enough to complicate the investigation of damage morphology. For that reason, the analysis of damage morphology is limited to cluster-free films. As a final step, a 90-nm-thick HfO_2 cupping layer was deposited by EBD, making the total HfO_2 film's optical thickness equal to 1 wave.

Absorption of HfO_2 thin films with embedded Hf nanoclusters stems from two sources: intrinsic absorption from not-yet-identified localized absorbing defects and absorption by artificially introduced Hf particles. In order to evaluate the latter contribution in the background-free environment, 355-nm absorption-free SiO_2 thin-film samples with embedded Hf particles were also prepared (Fig. 2(c)) using 10-nm Hf film TTFA. Hf particles were deposited on fused-silica substrates using ablation conditions identical to those described above for the HfO_2 host material. TEM witness samples showed Hf cluster size and areal-density distributions in SiO_2 very similar to HfO_2 samples (Fig. 4). As a final step, a 100-nm-thick SiO_2 cupping layer was deposited by EBD.

PHI is a photothermal pump/probe technique that uses a modulated pump beam for local modulated heating of the material and a probe beam that experiences scattering while passing through the heated volume. In the case of PHI (Fig. 5(a)), both pump and probe beams are focused into an overlapping, very tight, preferably diffraction-limited spot inside the material. A very small absorbing defect, being covered by such a spot, heats up and also, via heat conduction, causes the temperature T to rise in the surrounding host material. This process leads to the host refractive index n variation according to $n = n(T)$ and consequently probe-light scattering. Moreover, because of scatterer-size modulation, probe laser frequency ω is shifted by an amount equal to the modulation frequency Ω. Following the description given in Ref. [5], interference between scattered and propagating (or reflected, for back configuration) probe light in the far field creates a beat signal with an intensity $I(\Omega)$ proportional to light intensities of both the pump and probe beams:

$$I(\Omega) \sim I_{\text{pump}} I_{\text{probe}} n (\partial n/\partial T) \lambda^{-2} w^{-1} F(\Omega), \quad (1)$$

where I_{pump} and I_{probe} are pump and probe intensities, λ and w are the probe wavelength and beam waist,

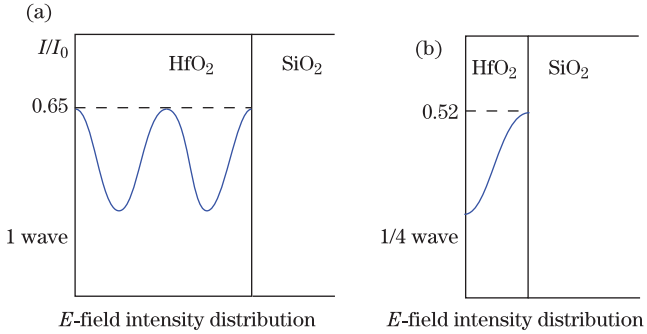

Fig. 3. 355-nm E-field intensity distribution for (a) 1-wave-thick and (b) 1/4-wave-thick HfO_2 samples.

respectively, and $F(\Omega)$ is a function describing heat conduction.

The experimental setup for PHI is shown in Fig. 5(b). A diode-pumped, continuous-wave (CW) semiconductor laser operating at 355-nm, 40-mW maximum output power (6 mW on sample) served as a pump laser, and a He–Ne laser operating at 633-nm, 10-mW maximum output power (5 mW on sample) was used as a probe. An acousto-optic modulator provided pump modulation at a frequency of 350 kHz. Pump and probe beams were combined at the entrance of the 40×/0.95-numerical aperture (N.A.) microscope objective focusing both beams onto the sample mounted on the nanopositioning stage that had a minimum lateral step size of 10 nm and a maximum scan size and axial displacement of 200 and 20 μm, respectively. Modulated probe light can be collected either by the same objective (back configuration) or, as was done in this work, by an additional lens (forward configuration). The detection system consists of a fast photodiode (PD), a lock-in amplifier (30-ms integration time), and a LabView-based data acquisition system. Reference [6] provides a detailed theoretical analysis of signals detected in either configuration.

Pump- and probe-beam focus spots were characterized using a 1-μm pinhole in the metal foil. A cross-sectional profile of the pump and probe beams' combined focal spot gave a full-width-at-half-maximum (FWHM) value of 0.79 μm, which should be considered as an upper limit based on the transfer function of the pinhole. We estimate the real FWHM value as ∼0.7 μm. Using this beam size and maximum UV power of 6 mW on the sample, we obtained maximum power densities on the sample of ∼1.6 MW/cm^2. To calibrate the system's spatial resolution and sensitivity, we used from 5- to 14-nm-diam isolated gold nanoparticles embedded inside SiO_2 film[8]. Figure 6(a) presents a 6-μm PHI scan and cross-sectional data for a sample with 14nm particles, which show that a single particle is imaged as a feature with a FWHM = 0.42 μm. Another example of system resolution is given by PHI imaging of multilayer-based dielectric diffraction grating with a 570-nm period (see Fig. 6(b)). These results proved both the true submicron spatial resolution and high sensitivity of the system. The setup response in the case of homogeneous absorption was calibrated using 200-nm-thick TiO_2 film (49% transmission at 355 nm) deposited on a fused-silica substrate. With a measured noise level of 0.5 μV and a detected maximum PHI signal of ∼6 000 μV, the signal-to-noise ratio (SNR) was $>10^4$.

Laser-damage studies were performed using 351-nm, 0.5-ns pulses from a Nd-doped glass laser. Damage thresholds (1-on-1 mode) were measured using 110×-magnification dark-field microscopy, and damage morphology was investigated by means of AFM and PHI.

Photothermal maps of standard HfO_2 films (not containing embedded Hf clusters) showed PHI signals with SNR >30 but did not show any structure pointing to the presence of localized absorbers. This suggests that the average distance between absorbers is much smaller than the ∼0.4-μm spatial resolution of the system. A comparison of the PHI signals for 1-wave- and 1/4-wave-thick films gave a ratio very close to 4:1, which also corresponds to the film thickness and absorbing volume ratios. This result points to a negligible contribution of the HfO_2/SiO_2 interface to the overall absorption despite the presence of an E-field intensity peak at this interface (see Fig. 3).

PHI mapping of HfO_2 films with embedded Hf particles showed strong signals from isolated large particles (see Fig. 7(b)) with an estimated smallest-detectable single-particle size of ∼15 nm. A comparison of the PHI background signal from spaces between large particles, where numerous from 1- to 5-nm–sized particles should be located (see Fig. 4), with signals from standard 1-wave-thick HfO_2 samples did not show any measurable differences (see Fig. 7(d)). In addition, no PHI signal was detected from small particles in the SiO_2 sample (see Fig. 7(c)) free from any background absorption at 355 nm. Assuming that the PHI signal is proportional to the number of absorbers within the pump beam's cross section in the film, the small clusters would require areal densities of least two orders of magnitude higher in order to attribute measured PHI signals in 1-wave HfO_2 films to the absorption by small clusters. This would lead to highly unrealistic areal densities corresponding roughly to the formation of ∼3-nm-thick metallic film. If these clusters would be distributed homogeneously inside the 180-nm-thick film, that would be equal to an excessive Hf atomic concentration of $\sim 10^{20}$ cm^{-3}—also too high for good-quality films. One reason that small particles are not generating a detectable PHI signal could be a poor thermal contact with the porous host material. If this is the case, we should assume that absorbing defects responsible for PHI signals in the standard (undoped) HfO_2 films have very good thermal contact with the host and, most probably, constitute an integral intrinsic part of the columnar film structure. High-density electronic defect areas, especially at the grain boundaries, can serve as such localized absorbers with good thermal contact. Electronic energy levels of oxygen-ion vacancy defect states V^+ and V^{2+} inside the HfO_2 bandgap (see Fig. 1) are high enough to permit free-electron formation by absorption of 355-nm, 3.5-eV photons. In the context of laser damage, further heating of these electrons by a laser pulse leads to electron avalanche formation and damage.

One possible route leading to such electronic defect formation may be linked to the presence in the evaporation plume of molecular species in the form of dimers and trimers. For instance, the presence of Hf_2 dimers with

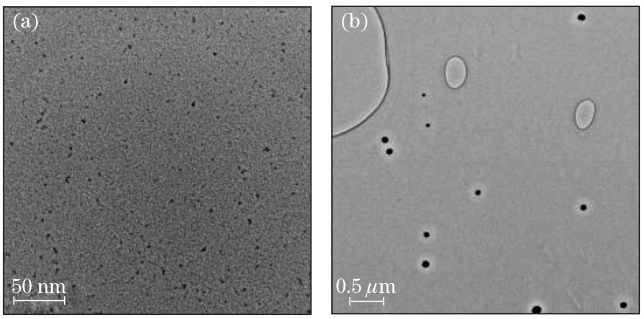

Fig. 4. TEM images of the Hf clusters deposited by TTFA of 10-nm-thick Hf metal film: (a) 350 × 350 (nm) image of small, from 1- to 5-nm–sized clusters; (b) 5 × 5 (μm) image showing large Hf clusters.

a yield relative to the atomic yield of $\sim 10^{-2}$ has been reported for 1-kV Ar^+ ion-beam sputtering of the Hf metallic targets[9]. Incorporation of the Hf_2 dimer into the HfO_2 matrix should be manifested by some kind of electronic defect formation. Still, first-principal calculations may be required to predict whether it will generate absorption in the near-UV.

Laser damage in 1-wave-thick standard HfO_2 films showed (AFM and PHI analysis) damage morphology in the form of nanometer- and few-micrometer–scale craters (Fig. 8). AFM measurements of the crater depth (Fig. 9) gave an average value of 186 nm, very close to the 180-nm thickness of the HfO_2 layer, indicating HfO_2-layer removal. This finding is in good agreement with PHI images where craters appear as dark (no signal) features (Figs. 8(a) and (c)). PHI images taken from the heavier-damaged central part of the damage site, as depicted in Fig. 8(c), also show enhanced absorption in the remaining portions of the HfO_2 film, indicating structural film modification from fast heating and cooling during the damage event. It allows one to forecast damage propagation under subsequent pulsed irradiation. AFM imaging (Fig. 10) also revealed that craters are missing the granular structure of the surrounding coating material, which indicates the SiO_2 material has reached the melting point $T_m(SiO_2) = 1\,986$ K at the bottom of the crater (note that the HfO_2 layer has been removed), material flow, and resolidification. The morphology of crater boundaries and bridges between craters also shows much less granularity, pointing to early stages of HfO_2 material melting ($T_m(HfO_2) = 3\,085$ K). On the other hand, crater edges are missing the elevated smooth rim typical of molten-material flow, indicating that HfO_2 material removal proceeds without full melting, via a stress-driven mechanism. One of the most-important features of the crater morphology is the presence of nanoscale protrusions in the central part of craters that can propagate from 30 to 80 nm into the SiO_2 layer (see Fig. 9). These protrusions indicate localized absorption and material removal in the SiO_2 layer, which suggests the effective transformation of SiO_2 into an absorptive material during some stages of the damage process. A possible scenario, illustrated in Fig. 11, may involve initial energy absorption and local temperature rise at random locations within the HfO_2 layer, including locations adjacent to the SiO_2 layer. Because of the inhomogeneous, porous structure of the coating, effective heat transfer at the HfO_2/SiO_2 interface and temperature rise in the SiO_2 material will take place only in selected nanoscale areas with better mechanical/thermal contact. At these selected locations, the temperature within the time frame of the laser pulse may reach the SiO_2 melting point or higher and, as demonstrated earlier[10], upon reaching $T \sim 2\,200$ K, may trigger the conversion of SiO_2 into an effectively absorbing material at 351 nm. Subsequent energy acquisition from the laser pulse will cause further temperature and pressure rise finalized by the explosive removal of the HfO_2 material within the crater volume and SiO_2 material within the central nanocrater. Such a damage mechanism might be relevant to any multilayer coatings comprised from HfO_2/SiO_2 pairs and designed for near-UV pulsed-laser applications. With an increase in laser fluence, the number of initiation points

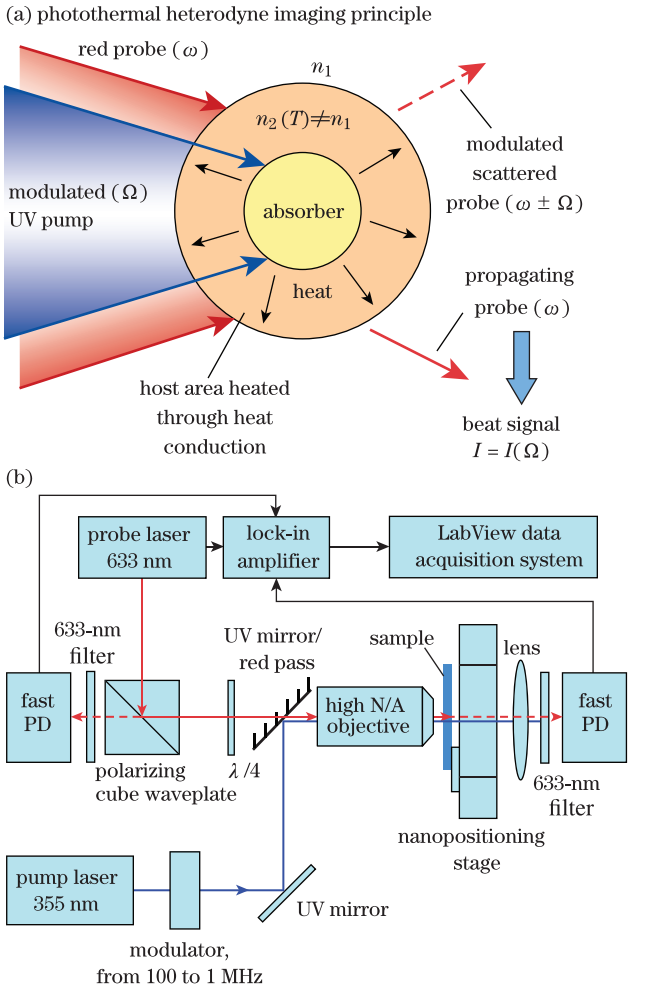

Fig. 5. Schematics of the (a) photothermal heterodyne signal formation and (b) PHI setup.

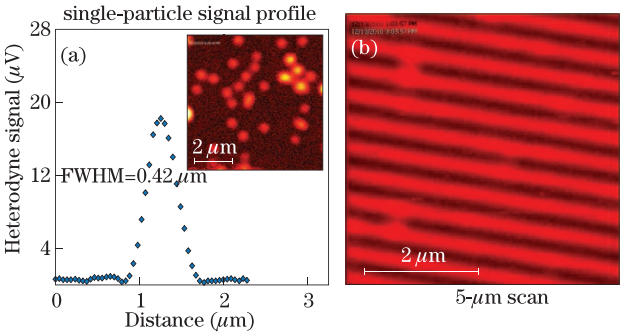

Fig. 6. Characterization of the PHI resolution: (a) single 14-nm gold particle signal profile; the inset shows a 6 × 6 (μm) image of 14-nm gold particles embedded in SiO_2; (b) 5 × 5 (μm) PHI image of multilayer-based holographic grating with resolved 570-nm period.

also increases, which is accompanied by the merging of damage craters (Fig. 10). The calculation of the average initiation-point separation using data from Fig. 10 gave a value of 272±59 nm. Taking into account that only part of the localized absorbers in HfO_2 can effectively transfer energy to the SiO_2 matrix, the actual average absorbing defect separation may be much smaller than measured initiation-point separation. The fact that even 45-nm-thick standard HfO_2 films generate large-enough

PHI signals strongly supports this conclusion and allows one to very conservatively estimate the upper limit of average absorber separation as $\leqslant$100 nm.

The results of this study point to possible venues to explore for improving laser-damage resistance of near-UV coatings for nanosecond-pulsed–laser applications. One, which is not new and still very important, is to reduce E-fields at the HfO_2/SiO_2 interfaces and consequently reduce energy deposition in the SiO_2 layer. Another suggestion is related to the porosity of deposited films. Increased porosity should reduce thermal contact and the rate of heat transfer at the interfaces. Recent experiments with ultraslow EBD of HfO_2 monolayers[11] with high porosity showed improved 351-nm, 0.5-ns damage thresholds. Of course, other considerations such as increased deposition time and environmental coating stability set some limits for the porosity increase. Use of the alternative high-index oxide materials with the larger bandgap E_B, as Sc_2O_3 ($E_B = 6$ eV) and especially Al_2O_3 ($E_B = 8.8$ eV), may be beneficial if it leads to an increase in the minimum photon energy required for free-electron formation. In this case, issues to be resolved are related to the stability of the deposition process for these materials. Finally, despite very limited options, an alternative low-index material with a large-enough bandgap and a melting point higher than the melting point for SiO_2 is also worthy of consideration.

In conclusion, near-UV absorption sources and ns-pulse damage mechanisms in coatings comprised from HfO_2/SiO_2 pairs are studied using HfO_2 monolayers deposited by e-beam evaporation on fused-silica substrates with an isolating SiO_2 film layer. Absorption in HfO_2 monolayers with and without artificially embedded Hf metal clusters is investigated using photothermal heterodyne imaging. The study shows that

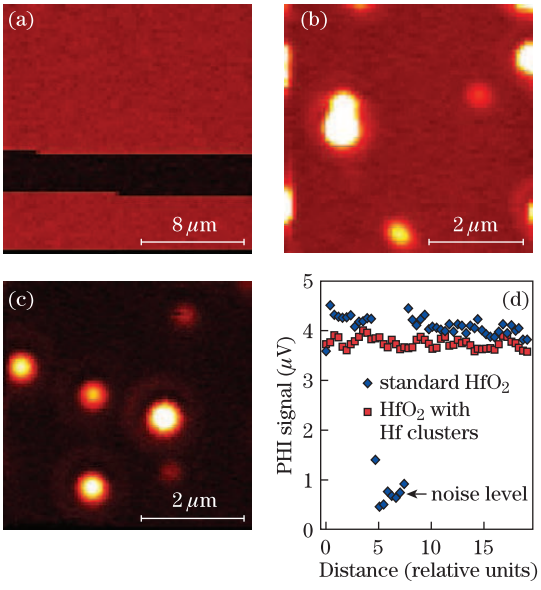

Fig. 7. PHI images of HfO_2 samples (a) without and (b) with Hf particles. (c) PHI image of SiO_2 sample with Hf particles. (d) PHI linear signal profiles taken from (a) and from large particle-free areas of (b). Note the absence of any signal in SiO_2 sample areas between large particles. The dark horizontal band in (a) corresponds to a measurement of the noise level by turning off the pump laser.

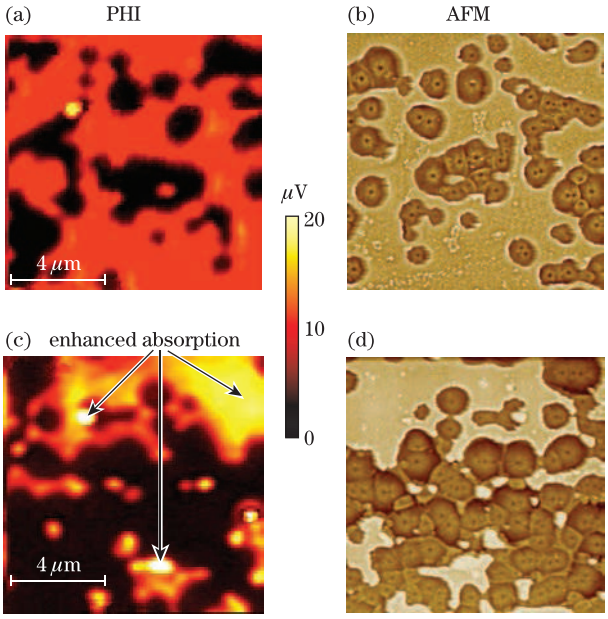

Fig. 8. (Color online) PHI and AFM images (10 × 10 (μm) scans) of 351nm, 0.5-ns damage morphology in HfO_2 standard (no Hf particles) sample. (a) and (b) correspond to the periphery of the damage site and laser fluence close to the threshold fluence. (c) and (d) are taken in the central part of the damage site characterized by higher fluence and show morphology dominated by merging craters. (c) clearly shows enhanced absorption in the remaining HfO_2 film.

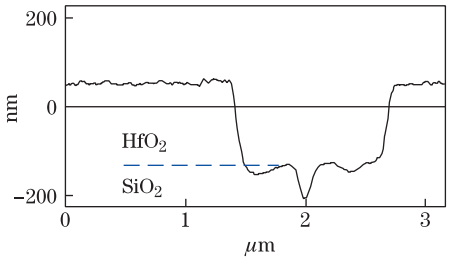

Fig. 9. Cross-sectional AFM profile through an isolated damage crater. Crater-depth measurement points to the removal of the HfO_2 layer. Central protrusion propagating into the SiO_2 layer points to the light absorption in the SiO_2 layer on some stage of the damage event.

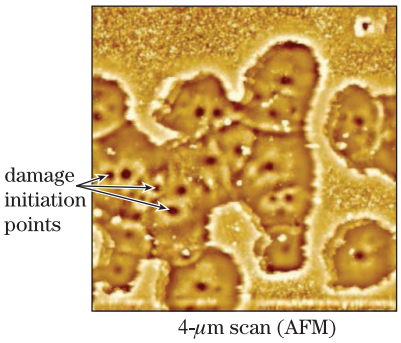

Fig. 10. AFM image of damage morphology shows smooth, glassy structure at the crater bottom, indicative of reaching the SiO_2 melting point. Partial smoothing of the crater boundaries also points to the early stages of melting in HfO_2 material. Numerous nanoscale protrusions visible inside the merging craters make it possible to estimate the average damage-initiating localized-absorber separation.

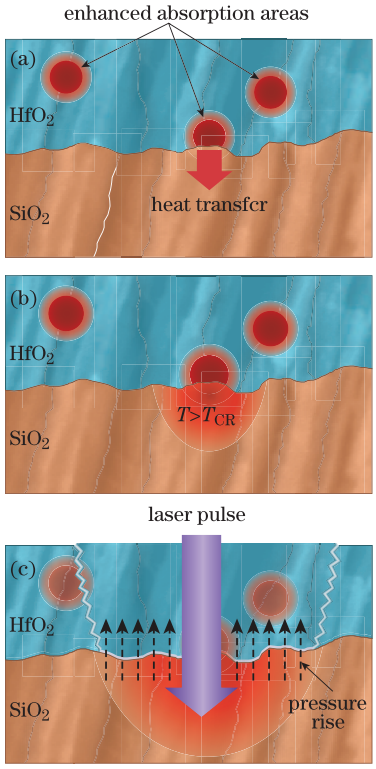

Fig. 11. Schematic presentation of the damage mechanism. (a) The process starts with localized absorption and temperature rise within the HfO_2 layer and is followed by heat transfer to the supporting SiO_2 layer. (b) At locations with good thermal contact, the temperature in SiO_2 can exceed critical temperature $T \sim 2\,200$ K, at which SiO_2 transforms into effectively absorbing material. (c) As a result, energy acquisition from laser pulse leads to quick temperature and pressure rise, explosive material removal, and damage.

from 1- to 5-nm-sized metal clusters with an areal density as high as $10^3 \mu m^{-2}$ but loosely bound to the columnar film structure cannot explain absorption measured in both doped and undoped films. This leads us to conclude that localized absorption is generated by the defects that constitute an integral intrinsic part of the columnar film structure. High-density areas of electronic defects, especially at the film grain boundaries, may be a good candidate for being the source of such localized absorption.

AFM and PHI damage morphology analysis allows us to suggest a damage mechanism for HfO_2 film supported by a SiO_2 layer. The process involves initial energy deposition and temperature rise in the HfO_2 layer followed by heat transfer to the supporting SiO_2 layer. At selected interfacial locations characterized by good thermal contact, the temperature in SiO_2 can reach a critical temperature $T \sim 2\,200$ K at which SiO_2 transforms into an effectively absorbing material for 351-nm photons. As a result, energy remaining in the laser pulse is effectively deposited in the SiO_2 layer, leading to quick temperature and pressure rise, explosive material removal, and damage. Such a damage mechanism mag be universal for any coating comprised from HfO_2/SiO_2 pairs and designed for near-UV, nanosecond-pulsed–laser applications. Based on such damage mechanism, possible modifications to coating designs and desirable high- and low-index material properties are suggested for improving laser-damage performance.

The author acknowledges E. Shin for Hf cluster deposition. This work was supported by the U.S. Department of Energy (DOE) Office of Inertial Confinement Fusion under Cooperative Agreement No. DE-FC52-08NA28302, the University of Rochester, and the New York State Energy Research and Development Authority. The support of DOE does not constitute an endorsement by DOE of the views expressed in this letter.

References

1. S. Papernov and A. W. Schmid, J. Appl. Phys. **82,** 5422 (1997).
2. A. S. Foster, F. L.Gejo, A. L. Shluger, and R. M. Nieminen, Phys. Rev. B **65,** 174117 (2002).
3. C. J. Stolz and F. Y. Génin, *Optical Interference Coatings* N. Kaiser and H. K. Pulker, (eds.) (Springer, Berlin, 2003) p. 309.
4. S. Papernov, A. W. Schmid, A. L. Rigatti, J. B. Oliver, and J. D. Howe, Proc. SPIE **5991,** 59911D (2005).
5. S. Berciaud, L. Cognet, G. A. Blab, and B. Lounis, Phys. Rev. Lett. **93,** 257402 (2004).
6. S. Berciaud, D. Lasne, G. A. Blab, L. Cognet, and B. Lounis, Phys. Rev. B **73,** 045424 (2006).
7. P. T. Murray and E. Shin, Proc. SPIE **7404,** 74040F (2009).
8. S. Papernov, A. Tait, W. Bittle, A. W. Schmid, J. B. Oliver, and P. Kupinski, J. Appl. Phys. **109,** 113106 (2011).
9. W. Gerhard and H. Oechsner, Z. Phys. B **22,** 41 (1975).
10. J. Bude, G. M. Guss, M. Matthews, and M. L. Spaeth, Proc. SPIE **6720,** 672009 (2007).
11. J. B. Oliver, S. Papernov, A. W. Schmid, and J. C. Lambropoulos, Proc. SPIE **7132,** 71320J (2008).